Realistic shell model and nuclei around ^{132}Sn

A. Gargano[1,*] and G. De Gregorio[1,2]

[1]Istituto Nazionale di Fisica Nucleare, Complesso Universitario di Monte S. Angelo, Via Cintia - I-80126 Napoli, Italy
[2]Dipartimento di Matematica e Fisica, Università degli Studi della Campania "Luigi Vanvitelli", viale Abramo Lincoln 5 - I-81100 Caserta, Italy

Abstract. This contribution reports on a shell-model study of nuclei in the ^{132}Sn region employing a realistic effective interaction derived from the CD-Bonn nucleon-nucleon potential renormalized through the use of the $V_{\mathrm{low-k}}$ approach. We shall focus on some selected results for nuclei with a few valence particles and/or holes with respect to ^{132}Sn, namely Sn isotopes with N > 82 and ^{130}Te, which have, in part, been discussed in previous papers. Results are compared with experiments, and predictions that may provide guidance to future experiments are also discussed. It is the aim of this contribution to underline the importance of studying ^{132}Sn neighbours to acquire a deep understanding of nuclear structure, that may be very useful also in other physics fields, and to show that the realistic shell model is a very effective tool to conduct these studies.

1 Introduction

During the last decade, nuclei in the mass region of ^{132}Sn have been the subject of extensive experimental studies and new spectroscopic data have been made available, although there are still some open questions, whose answer certainly requires further investigations.

The robustness of the N = 82 shell closure has been clearly shown by the mass measurement of [1], transfer reactions experiments [2] illustrating the single-particle nature of the levels in ^{133}Sn, as well as by other experimental results (see, for instance, [3, 4]).

Nuclei around ^{132}Sn represent a crucial opportunity to investigate the evolution of the shell structure around a heavy, neutron rich doubly-closed shell nucleus far-off stability. In the light- and medium-mass regions, structural changes have been evidenced for nuclei with a large excess of neutrons, leading to the breakdown of the traditional magic numbers and the appearance of new ones. These findings have driven a great theoretical effort to understand the microscopic mechanism underlying the shell evolution, with special attention to the role of the different components of the nuclear force (see, for instance, [5]). It is of great interest to verify if peculiar properties, as those observed in lighter nuclei, may be also observed in the ^{132}Sn region.

Apart from the intrinsic importance to nuclear structure, this region plays a key role in the dynamics of the rapid neutron-capture process of nucleosynthesis, the so-called *r*-process, since some of these nuclei are acting as a bottleneck for the reaction flow. The unknown evolution of the shell structure in this region is one of the main sources of nuclear physics uncertainty in *r*-process calculations. Nuclei in this region may also impact on fundamental physical issues as the neutrinoless double-β decay. In fact, ^{130}Te and ^{136}Xe are currently considered candidates for the observation of this process in some large experimental collaborations, such as the CUORE Collaboration in Italy [6], the EXO-200 Collaboration in New Mexico [7] and the KamLAND-Zen collaboration in Japan [8].

From the theoretical point of view, the shell model represents a very useful framework to understand the structure of these nuclei providing a microscopic description of nuclear properties essentially based on the use of effective interactions. Nuclei in close vicinity of ^{132}Sn may be very helpful to test shell-model effective interactions and ascertain their capability to provide reliable predictions for nuclei still inaccessible for present experiments.

We have conducted several studies on nuclei of this region in terms of the so-called realistic shell model, where the employed shell-model effective interactions are derived from modern nucleon-nucleon potentials by means of many-body techniques (see [9] and references therein). This represents a more fundamental approach to the shell model since effective interactions microscopically derived from the free nuclear potential, without any phenomenological adjustments, are employed.

In the present work, we report a few examples of our realistic shell-model calculations, which have partially discussed in previous papers [10–12]. In particular, we shall focus on very neutron-rich even-even tin isotopes with N > 82, from A = 134 to 140. As a matter of fact, little is known about the first three isotopes, while no information is available for ^{140}Sn, owing to the present experimental difficulties to access such short-lived nuclei, These Sn isotopes with a large N/Z ratio, going from 1.68 to 1.80, give the opportunity to better understand the forces that bind the nucleons together in very extreme conditions. In this connection, the possible appearance of a new shell at

*e-mail: gargano@na.infn.it

N = 90 may be of great interest, in analogy to what happens in lighter nuclei, for instance at N = 28 in the Ca isotopes.

We will also discuss the spectroscopic properties of ^{130}Te, which as discussed above is a candidate for the observation of the zero-neutrino double-β decay. For this nucleus, whose β decay properties are shown in [12], we shall report the results of a more complete calculation, with effective transition operators derived within a microscopic approach consistent with that employed for the effective shell-model Hamiltonian. Our aim is, in fact, to evaluate the predictive power of our approach, without introducing any adjustable parameters, in order to verify the reliability of our predictions for still unknown quantities, such as the nuclear matrix element involved in the neutrinoless double-β decay.

The paper is organized as follows. In Sect. 2, we outline the theoretical framework of our approach and give some details about the derivation of the shell-model Hamiltonian. Section 3 is devoted to the presentation of the results of our calculations and to the comparison with the available experimental data. A summary and some concluding remarks are given in the last Section.

2 Theoretical framework

Within the shell model the complexity of nuclear many-body problem is simplified by considering the nucleus as composed of an inert core, made up of completely filled neutron and proton shells, plus the remaining nucleons - *valence nucleons* - that interact in a truncated model space spanned in general by a single major proton shell and/or a single major neutron shell above the inert core. All the shells above the model space are empty and constitute the external space.

The shell-model Hamiltonian is written as

$$H_{\rm eff} = H_0 + V\,. \tag{1}$$

where H_0 is the one-body component, which describes the independent motion of the nucleons, while V represents the two-body residual interaction between the valence nucleons in the chosen model space.

The shell-model Hamiltonian should account in an effective way for the neglected degrees of freedom, namely for the excitations of core particles into the model and external spaces as well as for the excitations of valence particles in the external space. In the large majority of shell-model calculations performed until the beginning of the 2000s, empirical Hamiltonians have been employed, by considering the single-particle (SP) energies of the one-body term and the two-body matrix elements of the residual interaction as free parameters, or by taking an analytical expression with adjustable parameters for the residual interaction. In both cases, parameters are fixed by fitting experimental data.

Large progress has been made in the last 20 years or so in deriving microscopic shell-model interactions from realistic free nuclear potentials, especially by means of many-body perturbation theory. These so-called realistic shell-model calculations have the great advantage to bridge the gap between the effective shell-model interactions and underlying nuclear forces, while no adjustable parameters are needed.

A detailed description of the approach we use to derive realistic effective Hamiltonians is reported in [13, 14]. Here we just give a sketch of our procedure, that is outlined in the following scheme

1. Choosing the realistic nuclear potential;
2. Determining the model space better tailored to study the system under investigation;
3. Deriving the effective shell-model Hamiltonian;
4. Constructing and diagonalizing the Hamiltonian to obtain energies and wave functions;
5. Calculating the physical observables such as electromagnetic transition probabilities, Gamow-Teller strengths, etc.

The starting point of a realistic shell-model calculation is the nuclear potential, that may contain two- and three-body components. The quantitative role of the latter has been highlighted especially for light nuclei with $A \leq 12$ [15]. Recently, notable efforts are being made to study its effects on medium mass nuclei (see [16] and references therein), but for heavy nuclei the problem is completely open and no calculations are available so far. We limit, here, to consider only the nucleon-nucleon (NN) component, $V_{\rm NN}$, of the nuclear potential.

It is worth mentioning that in general, owing to its strong short-range repulsive behaviour, $V_{\rm NN}$ cannot be used to derive effective interactions within the framework of perturbative approaches. To overcome this problem, use is made of low-momentum potentials. It is done by starting from a realistic model for $V_{\rm NN}$ and integrating out its high-momentum components, thus obtaining a smooth potential that preserves exactly the onshell properties of the original potential [17]. Alternatively, one can resort directly to a chiral potential based upon the effective field theory [18]. In both cases, these low-momentum potentials, $V_{\rm low-k}$, may be used as input in the derivation of the effective shell-model interaction without the need of any further renormalization.

We have then to define, taking into account the limits of the available computing devices, the most appropriate model space to investigate the nuclei we are interested in. To this end, an auxiliary one-body potential U is introduced, that generates a SP energy spectrum organized in shells. Then, the effective Hamiltonian, $H_{\rm eff}$, is derived making use of the well-known $\hat{Q}$ box-plus-folded-diagram method, with the $\hat{Q}$ box defined in terms of the unperturbed energy ϵ as

$$\hat{Q}(\epsilon) = PH_1P + PH_1Q\frac{1}{\epsilon - QHQ}QH_1P\,. \qquad (2)$$

where $H_1 = V_{\text{low-k}} - U$, the operator P projects onto the truncated shell-model space, and $Q = 1 - P$.

Within this approach, the effective Hamiltonian is written in terms of the $\hat{Q}$ box and its derivatives

$$H_{\text{eff}} = \sum_i F_i\,. \qquad (3)$$

with

$$\begin{aligned} F_0(\epsilon_0) &= \hat{Q}(\epsilon_0) \\ F_1(\epsilon_0) &= \hat{Q}_1(\epsilon_0)\hat{Q}(\epsilon_0) \\ F_2(\epsilon_0) &= [\hat{Q}_2(\epsilon_0)\hat{Q}(\epsilon_0) + \hat{Q}_1(\epsilon_0)\hat{Q}_1(\epsilon_0)]\hat{Q}(\epsilon_0)\,. \\ &\cdots \end{aligned} \qquad (4)$$

where $\hat{Q}_n(\epsilon_0)$ is defined as

$$\hat{Q}_n(\epsilon_0) = \frac{1}{n!}\left.\frac{d^n\hat{Q}_0(\epsilon)}{d\epsilon^n}\right|_{\epsilon=\epsilon_0}\,. \qquad (5)$$

ϵ_0 being the model-space eigenvalue of H_0.

Once the $\hat{Q}$ box and its derivatives are calculated, the effective interaction is obtained by summing the series in Eq. 3 using the Lee-Suzuki technique [19], which yields converged results after a small number of iterations. The calculation of the $\hat{Q}$ box is performed by using its perturbative diagrammatic expansion and including one- and two-body diagrams up to a finite order. One- and two-body diagrams up to third order in the interaction are reported in [14], where the convergence properties of the $\hat{Q}$-box expansion are discussed in detail.

In principle, H_{eff} depends on the number of valence particles and a specific Hamiltonian should be derived for each system. However, it is usually evaluated only for the two-valence-particle system. This means that we include in our Hamiltonian only one- and two-body terms and neglect higher-body terms that come into play for systems with more than two particles and arise from the interaction via the two-body force between valence nucleons and excitations outside the model space.

Within this framework, the SP energies of our shell-model Hamiltonian result from the sum of the eigenvalues of H_0 and the one-body contributions of H_{eff}, while the two-body contributions of H_{eff} give rise to the two-body residual interaction. It worth mentioning, however, that a subtraction procedure can be used, so as to retain only the two-body terms of H_{eff} , while the SP energies are taken from experiment. This approach, although less fundamental, enables to take into account implicitly the effects of three-body forces on the SP energies.

In concluding this section, it should be pointed out that a consistent calculation for the observables requires the use of effective transition operators derived within the same framework as the effective Hamiltonian. The formalism to construct these operators has been developed by Suzuki and Okamoto [20], who have extended the $\hat{Q}$ box-plus-folded-diagram method developed for the Hamiltonian to this end. A description of our procedure to calculate the effective transition operators, based on Suzuki and Okamoto method, can be found in [12].

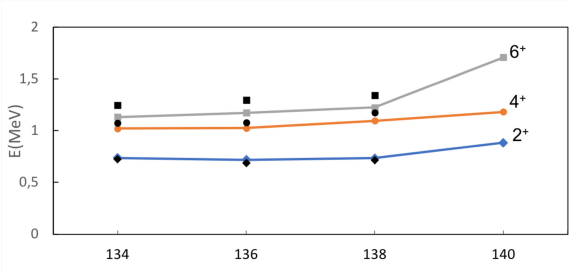

Figure 1. Calculated and experimental excitation energies (full black symbols) of the yrast 2^+, 4^+, and 6^+ states in tin isotopes with A = 134, 136, 138, and 140.

3 Results

As mentioned in the Introduction, we discuss here two cases, whose results have been partially reported in previous papers [10–12]. Our aim is to show the reliability of our approach as well as to illustrate some inconsistencies whose solution would require further investigations also from the experimental point of view.

In particular, we discuss the spectra and $E2$ transitions rates for Sn isotopes with $A = 136 - 140$. Then, we report on the spectroscopic properties of ^{130}Te. In both cases, the effective interaction is derived starting from the high precision CD-Bonn NN potential [21], renormalized by means of the $V_{\text{low-k}}$ approach, with $\Lambda = 2.2$ and $2.6\,\text{fm}^{-1}$ for Sn isotopes and ^{130}Te, respectively.

Calculations have been carried out using the shell-model code ANTOINE [22].

3.1 Sn isotopes with N > 82

We have considered the doubly magic ^{132}Sn as closed core and let the valence neutrons occupy the six levels $0h_{9/2}$, $1f_{7/2}$, $1f_{5/2}$, $2p_{3/2}$, $2p_{1/2}$, and $0i_{13/2}$ of the $82 - 126$ shell. Starting from the $V_{\text{low-k}}$, we have calculated the effective Hamiltonian by means of the $\hat{Q}$ box folded-diagram expansion, with the $\hat{Q}$ box including all diagrams up to second order in the interaction. In this case, as discussed in Sec. 2, we have employed a subtraction procedure so as to retain only the two body terms of H_{eff} , while the SP energies are taken from experiment. The $B(E2)$ values have been calculated using an effective neutron charge of $0.7e$, whose value is adjusted on the $B(E2; 6^+ \rightarrow 4^+)$ in ^{134}Sn.

The calculated excitation energies of the yrast 2^+, 4^+, and 6^+ states for ^{134,136,138,140}Sn are compared with the available experimental data [23–25] in Fig. 1, which points to a very good agreement between theory and experiment.

We predict an almost flat behavior for the energies of the three excited states, with a slight increase at N = 90 for the 2^+ and 4^+ states, which becomes more significant

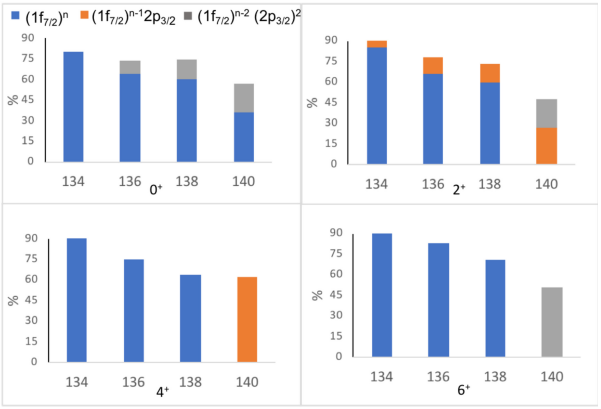

Figure 2. Percentages of the dominant configurations for the ground and the yrast 2^+, 4^+, 6^+ states in tin isotopes with A = 134, 136, 138, and 140.

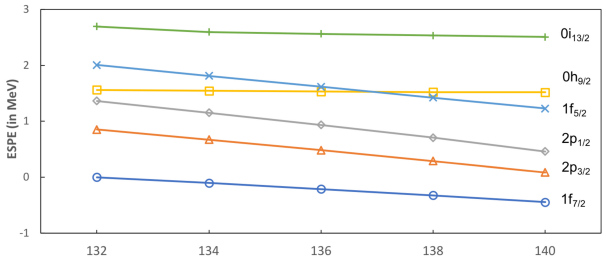

Figure 3. Effective single-particle energies of the orbitals of the $N = 82 - 126$ shell from A = 132 to 140.

for the 6^+ state. This behavior may be explained by the closure of the $1f_{7/2}$ orbital. In Fig. 2, we report the percentages of the main configurations for the ground and the yrast 2^+, 4^+, 6^+ states. It can be seen that all the states are dominated by the $(1f_{7/2})^n$ configuration up to ^{138}Sn, n being the number of valence neutrons. In ^{140}Sn, due to the filling of the $1f_{7/2}$ orbital, excited states derive essentially from neutron excitations to the $2p_{3/2}$ orbital, the 6^+ state requiring the excitation of at least two neutrons.

As a matter of fact, our results are in line with those of Ref. [26] and do not show a significant upshift of the 2^+ state in ^{140}Sn, which excludes the possible existence of a N = 90 shell closure in contrast to the conclusion of [28]. In [28], a large shell gap is found at N = 90 by using an empirical interaction or a realistic interaction with monopole corrections accounting for three body effects. These interactions produce, in fact, a considerable increase between the effective single-particle energies (ESPE) of the $1f_{7/2}$ and $2p_{3/2}$ orbitals when going from ^{132}Sn to ^{140}Sn. As it can be seen in Fig. 3, our effective single-particle energies do not show such an increase, but, on the contrary, indicate a slight decrease of about 100 keV.

Clearly, we cannot exclude that our results are affected by the omission of three-body forces. We have studied the contribution of chiral three-body forces to the monopole component of the effective shell-model Hamiltonian for nuclei belonging to fp shell in Ref. [16]. In this paper, we

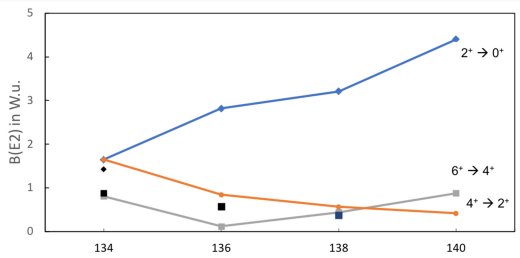

Figure 4. Calculated and experimental (full black symbols) $B(E2)$ strengths from the yrast 2^+, 4^+, and 6^+ states in tin isotopes with A = 134, 136, 138, and 140.

show that the inclusion of a three-body force leads to an enlargement of the gap between the $1f_{7/2}$ and $2p_{3/2}$ neutron ESPE of 0.7 MeV at N = 28, thus providing good closure properties in doubly-closed ^{48}Ca. However, even if these calculations point to the importance of taking into account three-body forces, they also indicate that their effect could not be so large as that predicted in [28] for ^{140}Sn. In any case, the above discussion points at the need of further theoretical investigations, as well as of acquiring more experimental data.

We discuss now the $E2$ transition properties of Sn isotopes under investigation. In Fig. 4 we have reported the $B(E2)$ values from the yrast 2^+, 4^+, and 6^+ states together with the available experimental data [23, 25, 27]. Unfortunately, no information are available for the $B(E2; 4^+ \to 2^+)$ transitions and the $B(E2; 2^+ \to 0^+)$ is known only for ^{134}Sn.

We see that the $B(E2; 2^+ \to 0^+)$ in ^{134}Sn and the $B(E2; 6^+ \to 4^+)$ in ^{138}Sn are well reproduced by the theory (the $B(E2; 6^+ \to 4^+)$ in ^{134}Sn is used to fix the neutron effective charge). On the other hand, the observed $B(E2; 6^+ \to 4^+)$ in ^{138}Sn is significantly underestimated. The predicted $B(E2; 6^+ \to 4^+)$ values are close to the seniority $v = 2$ pattern, namely to a symmetric positive parabola with the minimum value at N = 86 corresponding to a half-filled $1f_{7/2}$ orbital. The experimental behaviour shows a substantial deviation from the seniority scheme.

As a matter of fact, the calculated spectrum of ^{136}Sn, shows two 4^+ states very close in energy, at 1.020 and 1.180 MeV, which are dominated, respectively, by the $v = 2$ and 4 component. This means that small changes in the two-body matrix elements of the shell-model interaction may produce mixed seniority 4^+ states with consequent changes in $B(E2; 6^+ \to 4^+)$ pattern. On this basis, we have modified the $J = 2$, 4, and 6 diagonal matrix elements of our interaction for the $(1f_{7/2}^2$ configuration by about 50 - 100 keV.

In Table 1 and 2 the available experimental data are compared with the excitation energies and the $B(E2)$ values in ^{136}Sn, obtained by the two calculations, without (Th1) and with (Th2) modified interaction matrix elements. It may be seen that the $B(E2; 6^+ \to 4^+)$ obtained with modified matrix elements is in very good agreement with the experimental value, and also the agreement for the excitation energies is slightly improved. Very similar

Table 1. Calculated and experimental excitation energies (in MeV) for ^{136}Sn.

J^π	Th1	Th2	Expt
0^+	0.0	0.0	0.0
2^+	0.737	0.658	0.688
4^+_1	1.020	1.054	1.079
4^+_2	1.180	1.176	
6^+	1.133	1.280	1.295

Table 2. Calculated and experimental $B(E2)$ strengths (in W.u.) for ^{136}Sn.

$J^\pi_i \to J^\pi_f$	Th1	Th2	Expt
$2^+ \to 0^+$	117	119	
$4^+_1 \to 2^+$	34	90	
$6^+ \to 4^+_1$	5	32	24(4)
$6^+ \to 4^+_2$	66	41	

results are found in [25], where a reduction of 150 keV was introduced for the $(1f_{7/2})^2$ diagonal and off-diagonal matrix elements to reproduce the $B(E2; 6^+ \to 4^+)$ in ^{136}Sn. It is clear, however, that a sound test of the two-body matrix elements of the interaction requires more experimental data, as for instance the $B(E2; 4^+_1 \to 2^+)$ in ^{136}Sn, whose predictions from Th1 and Th2 are very different.

3.2 ^{130}Te

In this Section, we report results for ^{130}Te that have been obtained with a completely microscopic calculation, without using any empirical input. In fact, both the effective shell-model Hamiltonian, SP energies as well as two-body matrix elements, and electromagnetic transition operators are derived within the many-body perturbative approach described above by including diagrams up to the third order.

Our aim is to show that such kind of calculations are able to reproduce quantitatively the spectroscopic properties of this nucleus, which, as mentioned in the Introduction, is considered a candidate for the observation of the neutrinoless double-β decay. As model space, we have taken the five neutron and proton orbitals of the 50 - 82 shell outside the doubly closed ^{100}Sn, namely $0g_{7/2}$, $1d_{5/2}$, $1d_{3/2}$, $2s_{1/2}$, and $0h_{11/2}$.

The calculated spectrum of ^{130}Te up to about 2 MeV is compared with the experimental one [29] in Fig. 5, while Tables 3 and 4 show the comparison of the calculated and experimental [29, 30] $B(E2)$ and $B(M1)$ strengths, respectively. The agreement is overall very good. The largest discrepancy between theoretical and experimental excitation energies is 250 keV for the third 2^+ state, while for all the other states it is below 170 keV. As concerns the electromagnetic properties, we see that the few certain experimental values are well reproduced by our calculations.

In Ref. [12] we have reported the Gamow-Teller strength distributions and the calculated nuclear matrix element of the two-neutrino double-β decay for ^{130}Te and compared them with the experimental data. As for the electromagnetic operators, the Gamow-Teller operator is

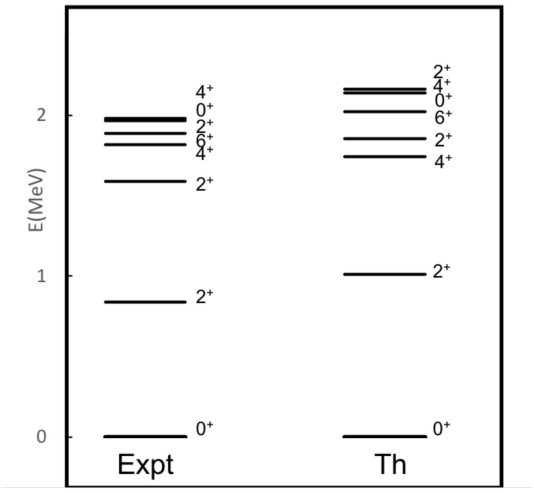

Figure 5. Experimental and calculated spectra for ^{130}Te

calculated within an approach that is consistent with the construction of the corresponding effective Hamiltonian. It is shown that also the decay properties of this nucleus are very well reproduced by the theory, without resorting to an empirical quenching of the axial coupling constant g_A.

Table 3. Calculated and experimental $B(E2)$ strengths (in W.u.) for ^{130}Te

$J^\pi_i \to J^\pi_f$	Th	Expt
$2^+_1 \to 0^+_1$	10.7	15.1(3)
$2^+_2 \to 2^+_1$	3.6	< 21(1)
		0.73(2)
$2^+_2 \to 0^+_1$	0.1	$< 1.3 \times 10^{-2}$(1)
$4^+_1 \to 2^+_2$	0.9	
$4^+_1 \to 2^+_1$	10.4	
$6^+ \to 4^+_1$	5.5	6.1(3)
$2^+_3 \to 4^+_1$	0.9	
$2^+_3 \to 2^+_2$	1.2	
$2^+_3 \to 2^+_1$	10.8	34(3)
		2.2(+3,-2)
$2^+_3 \to 0^+_1$	0.3	2.8×10^{-2}(4)

Table 4. Calculated and experimental $B(M1)$ strengths (in nm^2) for ^{130}Te

$J^\pi_i \to J^\pi_f$	Th	Expt
$2^+_2 \to 2^+_1$	0.085	$< 1.3 \times 10^{-2}$(1)
		4.3×10^{-2}(+2,-1)
$2^+_3 \to 2^+_2$	0.000	
$2^+_3 \to 2^+_1$	0.042	3.7×10^{-3}(+3,-4)
		9.7×10^{-2}(+8,-11)

4 Summary and Conclusions

In this contribution, we have presented results of realistic shell-model calculations for nuclei in the ^{132}Sn region.

This region is of great interest for studying the evolution of the shell structure - and how it is driven by the underlying nuclear forces - around a heavy, neutron-rich doubly closed-shell nucleus far off stability. It plays also a key role in the dynamics of the rapid neutron-capture process of nucleosynthesis and some nuclei near ^{132}Sn impact on fundamental physical issues such as the neutrinoless double-β decay. Relevant data are, however, still missing, but hopefully they can be provided by future experiments, thanks to the availability of radioactive ion beams of sufficiently high intensity.

We have employed effective interactions derived by many-body perturbation theory from the CD-Bonn nucleon-nucleon potential, whose short-range repulsion is renormalized by constructing a smooth low-momentum potential, $V_{\mathrm{low-k}}$. First, we have discussed results for very neutron-rich even-even N > 82 tin isotopes with A = 134 - 140, by employing realistic two-body matrix elements of the interaction and empirical SP energies as well as effective neutron charge. Then, we have reported excitation energies and electromagnetic properties of ^{130}Te obtained within a more consistent calculation, with a completely microscopic Hamiltonian and effective transition operators derived by using the same framework of the effective shell-model Hamiltonian. In latter case, our aim was to assess the predictive power of our approach, without introducing any adjustable parameters, in order to make predictions for still unknown quantities, as the nuclear matrix element involved in the neutrinoless double-β decay.

We have shown that realistic shell-model calculations are able to reproduce quantitatively the available experimental data of these nuclei, testifying that they are a very effective tool to investigate the nuclear structure properties of the ^{132}Sn region. Our discussion for Sn isotopes also points to some remaining open questions, that certainly need further investigations from both the theoretical and experimental points of view.

Acknowledments

The material presented here is based upon the work of the Nuclear Theory Group of Naples, to which L. Coraggio and N. Itaco have largely contributed.

References

[1] M. Dworschak, G. Audi, K. Blaum *et al.*, Phys. Rev. Lett. **100**, 072501 (2008).

[2] K. L. Jones, A. S. Adekola, D. W. Bardayan *et al.*, Nature (London) **465**, 454 (2010).

[3] A. E. Stuchbery, J. M. Allmond, A. Galindo-Uribarri *et al.*, Phys. Rev. C **88**, 051304(R) (2013) .

[4] J. M. Allmond, A. E. Stuchbery, J. R. Beene *et al.*, Phys. Rev. Lett. **112**, 172701 (2014).

[5] T. Otsuka, A. Gade, O. Sorlin *et al.*, arXiv:1805.06501

[6] K. Alfonso, D. R. Artusa, F. T. Avignone III *et al.* (CUORE Collaboration), Phys. Rev. Lett. **115**, 102502 (2015).

[7] M. Auger, D. J. Auty, P. S. Barbeau *et al.* (EXO Collaboration), Phys. Rev. Lett. **109**, 032505 (2012).

[8] A. Gando, Y. Gando, T. Hachiya *et al.* (KamLAND-Zen Collaboration), Phys. Rev. Lett. **117**, 082503 (2016).

[9] L. Coraggio, A. Covello, A. Gargano *et al.*, Phys. Rev. C **88**, 041304(R) (2013).

[10] A. Covello, L. Coraggio, A. Gargano *et al.*, J. Phys. Conf. Ser. **267**, 012019 (2011).

[11] L. Coraggio, L. De Angelis, T. Fukui *et al.*, Phys. Rev. C **95**, 064324 (2017).

[12] L. Coraggio, L. De Angelis, T. Fukui *et al.*, Phys. Rev. C **100**, 014316 (2019).

[13] L. Coraggio, A. Covello, A. Gargano *et al.*, Prog. Part. Nucl. Phys. **62**, 135 (2009).

[14] L. Coraggio, A. Covello, A. Gargano *et al.*, Ann. Phys. **327**, 2125 (2012).

[15] J. Carlson, S. Gandolfi, F. Pederiva *et al.*, Rev. Mod. Phys. **87**, 1067 (2015), and references therein.

[16] Y. Z. Ma, L. Coraggio, L. De Angelis *et al.*, Phys. Rev. C **100**, 034324 (2019).

[17] S. Bogner, T. T. S. Kuo, L. Coraggio *et al.*, Phys. Rev. C **65**, R051301 (2002).

[18] R. Machleidt and D. R. Entem, Phys. Rep. **503**, 1 (2011).

[19] K. Suzuki and S. Y. Lee, Prog. Theor. Phys. **64**, 2091 (1980).

[20] K. Suzuki and R. Okamoto, Prog. Theor. Phys. **93**, 905 (1995).

[21] R. Machleidt, Phys. Rev. C **63**, 024001 (2001).

[22] E. Caurier, G. Martínez-Pinedo, F. Nowacki *et al.*, Rev. Mod. Phys. **77**, 427 (2005).

[23] A. Korgul, W. Urban, T. Rząca-Urban *et al.*, Eur. Phys. J. A **7**, 167 (2000).

[24] H. Wang, N. Aoi, S. Takeuchi *et al.*, Prog. Theor. Exp. Phys. 2014, 023D02 (2014) .

[25] G. S. Simpson, G. Gey, A. Jungclaus *et al.*, Phys. Rev. Lett. **113**, 132502 (2014).

[26] M. P. Kartamyshev, T. Engeland, M. Hjorth-Jensen *et al.*, Phys. Rev. C **76** 024313 (2007).

[27] J. R. Beene, R. L. Varner, C. Baktash *et al.*, Nucl. Phys, A **746**, 471c (2004).

[28] S. Sarkar and M. S. Sarkar, Phys. Rev. C **81** 064328 (2010) and references therein.

[29] Data extracted using the NNDC On-line Data Service from the ENSDF database, file revised as of November. 26, 2019, URL https://www.nndc.bnl.gov/ensdf.

[30] Data extracted using the NNDC On-line Data Service from the XUNDL database, file revised as of November. 26, 2019, URL https://www.nndc.bnl.gov/ensdf/xundl.psp.

[31] S. F. Hicks, J. R. Vanhoy, and S. W. Yates, Phys. Rev. C **78**, 054320 (2008).